

$\pi^- \pi^+ \rightarrow \pi^- \pi^+$ interactions below 0.7 GeV from $\pi^- p \rightarrow \pi^- \pi^+ n$ data at 5 GeV/c

V. Srinivasan, J. A. Helland,* A. J. Lennox,† J. A. Poirier, J. P. Prukop,‡ C. A. Rey,
O. R. Sander,§ N. N. Biswas, N. M. Cason, V. P. Kenney, and W. D. Shephard

Department of Physics, University of Notre Dame, Notre Dame, Indiana 46556^{||}

R. D. Klem and I. Spirn

Argonne National Laboratory, Argonne, Illinois 60439[¶]

(Received 13 March 1975)

Magnetostrictive spark chambers were used with a large-aperture magnet spectrometer to study the reaction $\pi^- p \rightarrow \pi^- \pi^+ n$ at 5.0 GeV/c at Argonne National Laboratory. Differential cross sections for this reaction were measured in the region of low nucleon momentum transfer. Extrapolation techniques were used to obtain cross sections and phase shifts for the reaction $\pi^- \pi^+ \rightarrow \pi^- \pi^+$ in the region of dipion mass less than 0.7 GeV. Effects of the interference between the strong $\pi^- \pi^+$ amplitude and the Coulomb amplitude off the mass shell were investigated and were found to be small.

I. INTRODUCTION

There is at present no direct experimental method for studying the reactions $\pi\pi \rightarrow \pi\pi$. Hence, we choose to examine these fundamental interactions by studying the dipion system produced in the reaction $\pi^+ p \rightarrow \pi^+ \pi^+ n$. Using the assumption that these latter reactions are dominated by the one-pion-exchange mechanism (OPE), it is possible to relate the $\pi^+ p \rightarrow \pi^+ \pi^+ n$ cross section to the scattering of the beam pion by the exchanged virtual pion. For dipion masses below 0.7 GeV, $\pi^+ \pi^+ \rightarrow \pi^+ \pi^+$ scattering can be parameterized in terms of two phase shifts, δ_0^0 and δ_2^0 , using the notation δ_I^J , where I is the isotopic spin and J is the angular momentum. On the other hand, the $\pi^- \pi^+ \rightarrow \pi^- \pi^+$ scattering in the same energy region involves five phase shifts, namely, δ_0^0 , δ_2^0 , δ_1^1 , δ_2^1 , and δ_2^2 . The values of δ_0^0 and δ_2^0 are known from our study of the reaction $\pi^+ p \rightarrow \pi^+ \pi^+ n$. In the present paper we deduce values for δ_0^0 , δ_2^0 , and δ_1^1 using the reaction $\pi^- p \rightarrow \pi^- \pi^+ n$.

Data on the interaction $\pi^- p \rightarrow \pi^- \pi^+ n$ at 5 GeV/c were obtained in an experiment performed at the Zero Gradient Synchrotron of Argonne National Laboratory. This experiment used magnetostrictive spark chambers and a large-aperture magnet spectrometer to acquire data in the low-momentum-transfer region of the dipion system. The information thus obtained is presented in terms of the variables $M_{\pi\pi}$, Δ^2 , θ_J , and ϕ_{TY} , where $M_{\pi\pi}$ is the invariant dipion mass, Δ^2 is the square of the momentum transfer between the incoming proton and the outgoing neutron, θ_J is the angle between the incoming and outgoing pion in the dipion rest frame, and ϕ_{TY} is the Treiman-Yang angle between the scattering plane of the proton and neutron and the decay plane of the dipion system. The δ_0^0 , δ_2^0 , and δ_1^1 phase shifts for $\pi^- \pi^+ \rightarrow \pi^- \pi^+$ presented here are the results of an analysis of 33 295 $\pi^- p \rightarrow \pi^- \pi^+ n$ events. The kinematic regions investi-

gated in this study include all values of θ_J and ϕ_{TY} . The region where the cross section is dominated by the ρ resonance was excluded by restricting $M_{\pi\pi}$ to values less than 0.7 GeV. In order that the mass of the virtual exchange pion remain close to the pion rest mass, μ , we required $\Delta^2 < 8\mu^2$.

II. EXPERIMENTAL SETUP AND DATA REDUCTION

Figure 1 is an over-all plan view of the experiment. A detailed description of the equipment shown there, as well as the definition of the event trigger has already been presented.¹ The π^- beam for this experiment had a central value of 5.09 ± 0.03 GeV/c and a momentum spread of $\pm 0.5\%$. The μ^- and e^- contamination in the beam relative to π^- was 1.9% while the K^- contamination was negligible.

A total of 61 magnetic tapes with ~3.4 million event triggers were processed off-line. The track finding program, CRUNCH, identified tracks and found those topologies where one charged particle entered the hydrogen target and two charged particles left the target and passed through the magnet. Cuts were made on events whose vertices were outside the target and on events having more than two sparks in the chambers immediately downstream of the target.

The program, CIRCE,² did the geometrical fitting and calculated the complete error correlation matrix. It orbited the tracks through the nonuniform magnetic field, and for each track it found the momentum vectors which minimized the χ^2 of the fit to the spark data consistent with a common vertex constraint. This vertex was required to be within ± 7.11 cm from the center of the hydrogen target, a region slightly smaller than the length of the hydrogen target flask. A cut was also made on the total χ^2 .

The error correlation matrix calculated in

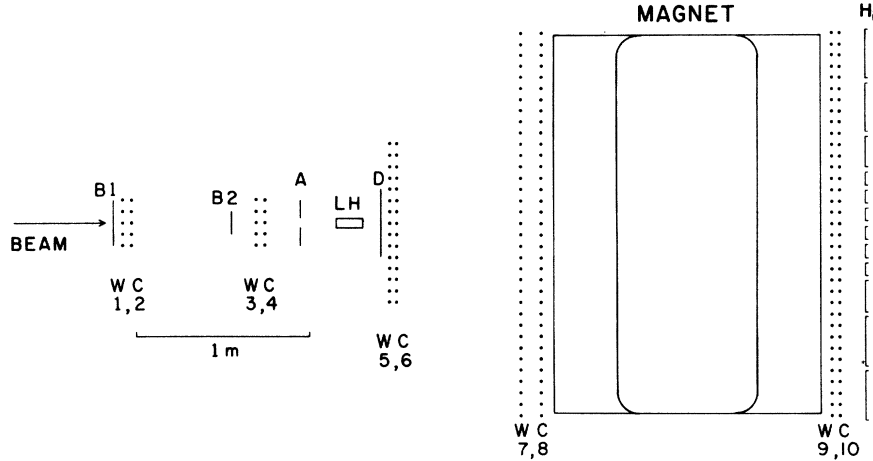


FIG. 1. Over-all plan view of the experiment. The dotted lines represent the position of magnetostrictive wire spark chambers, WC. The solid lines represent the locations of the scintillation counters $B1$, $B2$, A , and the dE/dx counter, D , used in the logic which triggered the spark chambers. The hydrogen target is labeled LH.

CIRCE was then used in the program, TEUTA,³ which calculated the kinematic fit probability, P , for various final-state hypotheses. In order to reduce the background contamination we required that $P(\pi^-p \rightarrow \pi^- \pi^+ n)$ be greater than twice $P(\pi^-p \rightarrow \pi^- p \pi^0)$ and that $P(\pi^-p \rightarrow K^- K^+ n)$ be less than 0.3.

We also studied the background by examining the square of the missing mass of the neutrals, MM^2 , which was calculated assuming that the two final-state charged tracks were pions. Figure 2 shows the values of MM^2 thus obtained from the data. The curves in Fig. 2 were obtained by generating Monte Carlo events and fitting their MM^2 distributions to the data. These Monte Carlo events included the signal (a) $\pi^-p \rightarrow \pi^- \pi^+ n$ and the backgrounds (b) $\pi^-p \rightarrow \pi^- p \pi^0$, (c) $\pi^-p \rightarrow \pi^- \pi^+ n \pi^0$, and (d) $\pi^-p \rightarrow K^- K^+ n$. All of these events were first processed by the geometrical weighting program, and their MM^2 was calculated assuming that the reaction was $\pi^-p \rightarrow \pi^- \pi^+ n$. After making the cut $0.68 \leq MM^2 \leq 1.0 \text{ GeV}^2$, we ascertained the backgrounds within this cut and the correction for the loss of good events falling outside the cut. The corrections applied to the data for these cuts as well as other corrections are listed in Table I.

III. RESULTS

A. Cross sections and distributions for $\pi^-p \rightarrow \pi^- \pi^+ n$

Table II contains our measurements of the $\pi^-p \rightarrow \pi^- \pi^+ n$ differential cross sections, $d^3\sigma/dM_{\pi\pi}d(\Delta')^2 \times d(\cos\theta_f)$, where $(\Delta')^2 = \Delta^2 - \Delta_{\min}^2$. For the 5 GeV/ c incident beam momentum of this experiment, Δ_{\min}^2 ranges from 0.00013 to 0.0078 $(\text{GeV}/c)^2$ for values

of $M_{\pi\pi}$ from threshold to 0.7 GeV. The differential cross sections in Table II reflect all the corrections and weighting factors listed in Table I, but with the correction listed in Table I (b) 1 made independently for each bin in $(\Delta')^2$ and $M_{\pi\pi}$. These cross sections were used directly in the analysis described in part C below. The same data divided into smaller $M_{\pi\pi}$ and $(\Delta')^2$ bins and integrated over $\cos\theta_f$ were used to perform the extrapolations discussed in part B.

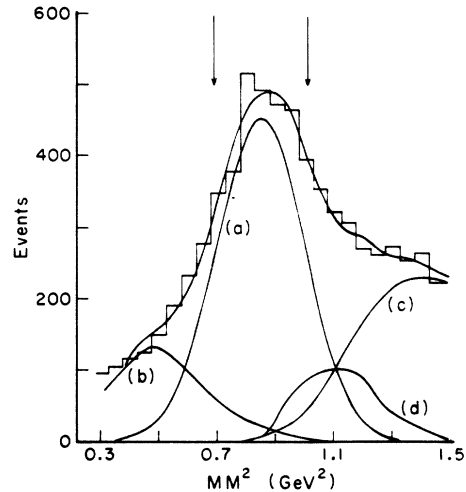


FIG. 2. Maximum-likelihood fits to the MM^2 plot for the data with the cuts of $(\Delta')^2 < 8\mu^2$ and $M_{\pi\pi} < 0.7 \text{ GeV}$. The relative amounts of each reaction inside the indicated cuts are (a) $\pi^-p \rightarrow \pi^- \pi^+ n = 2470$ events, (b) $\pi^-p \rightarrow \pi^- p \pi^0 = 190$ events, (c) $\pi^-p \rightarrow \pi^- \pi^+ n \pi^0 = 68$ events, and (d) $\pi^-p \rightarrow K^- K^+ n = 147$ events.

TABLE I. Summary of all corrections to the cross sections.

(a) Inverse of the weighting factors applied on an event-by-event basis	
	Range
1. Geometrical acceptance of apparatus	1.0 to 0.10
2. Interactions of secondary particles	0.98 to 0.90
3. Decay of secondary pions	0.96 to 0.85
(b) Inverse of the weighting factors applied to all events	
	Value
1. MM^2 and TEUTA χ^2 cuts, background contaminations	0.855 ± 0.020
2. Cut on CIRCE χ^2 parameter	0.970 ± 0.010
3. Chamber efficiencies	0.924 ± 0.012
4. Spark cut	0.692 ± 0.030
5. Ambiguities in track reconstruction	0.949 ± 0.020
6. μ and e contamination	0.981 ± 0.002
7. dE/dx trigger efficiency	0.940 ± 0.005
8. Empty-target effects	1.010 ± 0.005
9. Beam absorption in hydrogen target	0.990 ± 0.002
10. Effect of Coulomb scattering	1.000 ± 0.005
Net over-all systematic corrections	0.464 ± 0.026

The projections of the data in $M_{\pi\pi}$, $(\Delta')^2$, $\cos\theta_J$, and ϕ_{TY} are presented in Figs. 3 through 6. In each figure the lower histogram is the actual number of events while the upper one is the data weighted by the inverse of the geometrical acceptance, the pion decay probability, and the secondary interaction probability listed in Table I(a).

B. Extrapolation to $\pi^- \pi^+ \rightarrow \pi^- \pi^+$ on the mass shell

1. Determination of the on-mass-shell cross sections

Assuming the dominance of the one-pion exchange mechanism, one can relate the $\pi^- p \rightarrow \pi^- \pi^+ n$ cross section to the cross section for the scattering of a beam pion by the exchanged pion. This relationship is shown schematically in Figs. 7(a) and 7(b). In Fig. 7(b) the exchanged (virtual) pion is off the mass shell by an amount $\Delta^2 + \mu^2$. Chew and Low⁴ write the off-shell $\pi\pi$ cross section, " σ ", as

$$\frac{1}{\mu^2} \Delta^2 \sigma = \frac{4\pi P_L^2}{f^2 M_{\pi\pi}} \frac{(\Delta^2 + \mu^2)^2}{(M_{\pi\pi} - 4\mu^2)^{1/2}} \times \frac{d^2\sigma(\pi^- p \rightarrow \pi^- \pi^+ n)}{d\Delta^2 dM_{\pi\pi}^2}, \quad (1)$$

where $f^2 =$ twice the π^0 -nucleon coupling constant $= 2 \times 0.081$ and P_L is the beam momentum in the laboratory. As $\Delta^2 \rightarrow -\mu^2$ the mass of the virtual pion approaches that of a real pion, that is, the virtual pion comes closer to being on the mass shell. Thus, the on-mass-shell $\pi\pi \rightarrow \pi\pi$ cross section, $\sigma_{\pi\pi}$, is defined by an extrapolation:

$$\sigma_{\pi\pi} = \frac{-1}{\mu^2} \lim_{\Delta^2 \rightarrow -\mu^2} (\Delta^2 \sigma). \quad (2)$$

We applied (1) to our data, found the best fit of $\Delta^2 \sigma$ to three different functions of Δ^2 , and then extrapolated each function to $\Delta^2 = -\mu^2$. The three functional forms investigated were

$$\Delta^2 \sigma_i = \beta \Delta^2, \quad (3)$$

$$\Delta^2 \sigma_{ii} = \alpha + \beta \Delta^2, \quad (4)$$

$$\Delta^2 \sigma_{iii} = \alpha + \beta x, \quad (5)$$

where α and β are fitted parameters and

$$x = (c + d\Delta^2)/(e + \Delta^2). \quad (6)$$

Equation (3) requires that $(1/\Delta^2)d^2\sigma(\pi^- p \rightarrow \pi^- \pi^+ n)/d\Delta^2 dM_{\pi\pi}^2$ be finite at $\Delta^2 = 0$, or that $d^2\sigma(\pi^- p \rightarrow \pi^- \pi^+ n)/d\Delta^2 dM_{\pi\pi}^2$ vanish at $\Delta^2 = 0$. Forms (4) and (5) do not

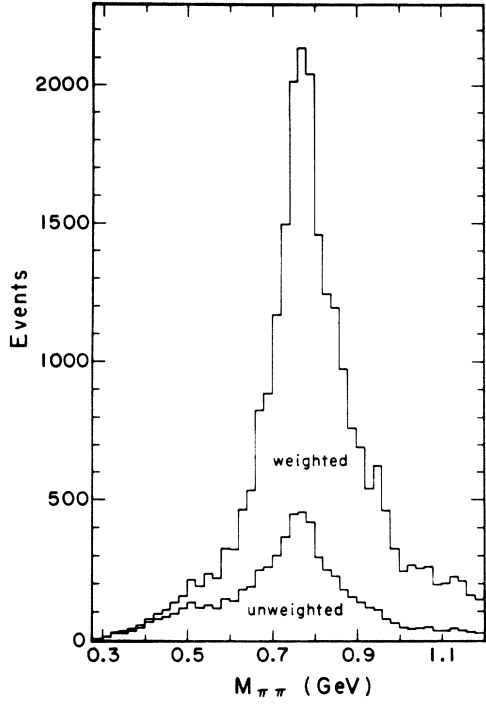


FIG. 3. The 6122 raw or 24 209 weighted $\pi^- p \rightarrow \pi^- \pi^+ n$ data events displayed in $M_{\pi\pi}$ bins of 0.02 GeV with a resolution of ~ 0.005 GeV. The following cuts have been applied: $0.68 < MM^2 < 1.0$ GeV², probability ($\pi^- p \rightarrow \pi^- \pi^+ n$) $>$ twice the probability ($\pi^- p \rightarrow \pi^- p \pi^0$), probability ($\pi^- p \rightarrow K^- K^+ n$) $<$ 30%, and $(\Delta')^2 < 8\mu^2$. For $M_{\pi\pi} \geq 0.8$ GeV, the weighted events are systematically low because of experimental biases not properly corrected by the correction factor of Table I (a)1. The analysis in this paper has been restricted to $M_{\pi\pi} < 0.7$ GeV; for this region a weighted event corresponds to $0.012 \mu\text{b}$.

have this constraint. Equation (6) is a conformal mapping which has been suggested⁵⁻⁷ to improve the convergence of the extrapolation. The curves shown in Fig. 8 were obtained using the form (5) and are presented as an example of an unconstrained fit.

Following the technique of Benecke and Dürre⁸ we define " σ_{BD} " = " σ " \times FF_{BD} , where $FF_{\text{BD}}(\Delta^2, M_{\pi\pi})$ approaches one as $\Delta^2 \rightarrow -\mu^2$. Table III summarizes the results of the extrapolations with and without the use of the form factor for the three different functional forms, Eqs. (3)–(5). This table presents the extrapolated $\pi^- \pi^+ \rightarrow \pi^- \pi^+$ on-mass-shell cross sections, the χ^2 of the fits, and the values of $\Delta^2 \sigma$ at $\Delta^2 = 0$ for each of the six fits. The values for the on-shell cross sections depend systematically on the choice of the functional form and the choice of a form factor, although the relative shapes are similar. The smaller errors obtained by using form (3) are due to the strong constraint

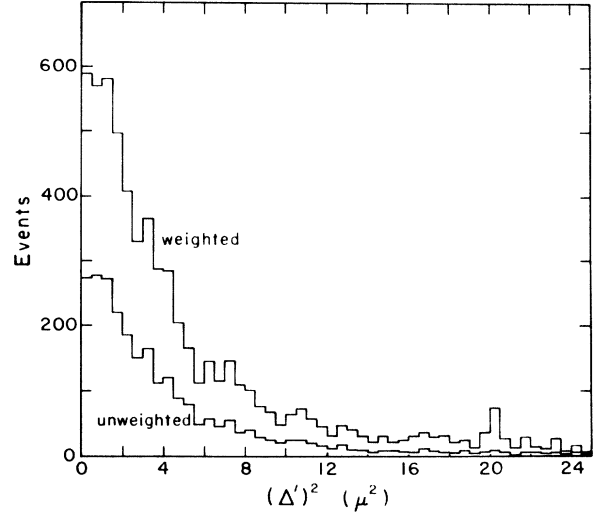


FIG. 4. The 2561 raw or 6133 weighted $\pi^- p \rightarrow \pi^- \pi^+ n$ data events displayed in $(\Delta')^2$ bins of $0.5\mu^2$ with a resolution of $\sim 0.1\mu^2$. The following cuts have been applied: $0.68 < MM^2 < 1.0$ GeV², probability ($\pi^- p \rightarrow \pi^- \pi^+ n$) $>$ twice the probability ($\pi^- p \rightarrow \pi^- p \pi^0$), probability ($\pi^- p \rightarrow K^- K^+ n$) $<$ 30%, and $M_{\pi\pi} < 0.7$ GeV. A weighted event with $(\Delta')^2 < 8\mu^2$ corresponds to $0.012 \mu\text{b}$.

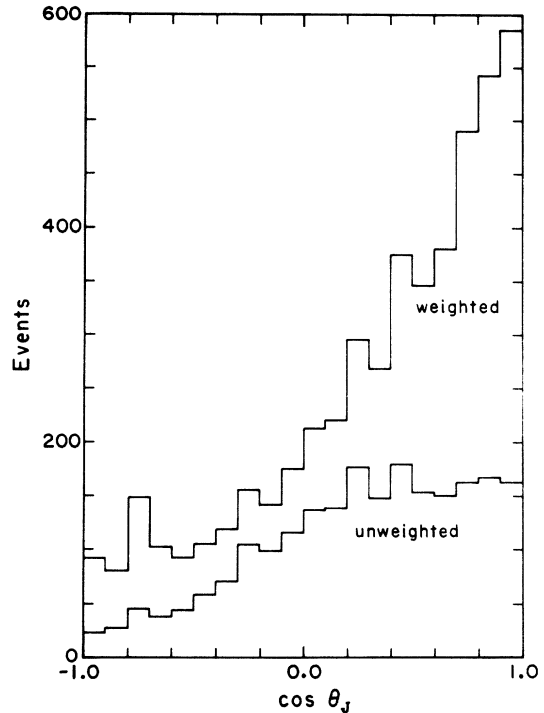


FIG. 5. The 2196 raw or 4920 weighted $\pi^- p \rightarrow \pi^- \pi^+ n$ data events displayed in $\cos\theta_j$ bins of 0.1 with a resolution of ~ 0.01 . The following cuts have been applied: $0.68 < MM^2 < 1.0$ GeV², probability ($\pi^- p \rightarrow \pi^- \pi^+ n$) $>$ twice the probability ($\pi^- p \rightarrow \pi^- p \pi^0$), probability ($\pi^- p \rightarrow K^- K^+ n$) $<$ 30%, $M_{\pi\pi} < 0.7$ GeV, and $(\Delta')^2 < 8\mu^2$. A weighted event corresponds to $0.012 \mu\text{b}$.

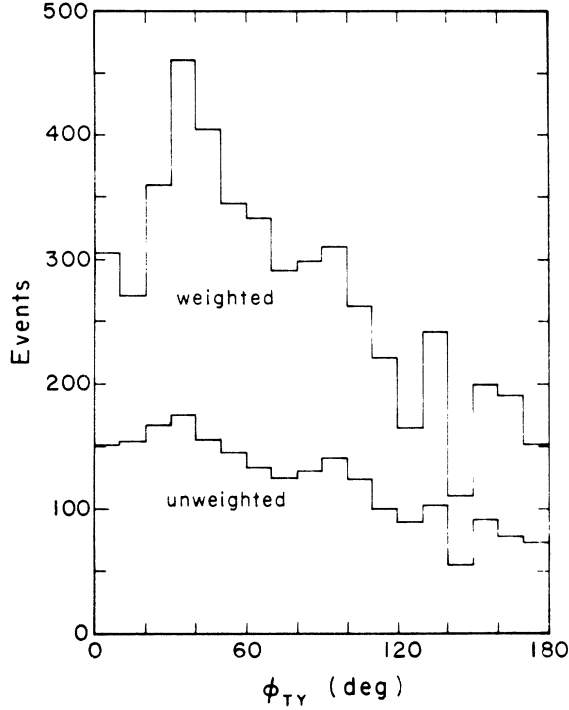


FIG. 6. The 2196 raw or 4920 weighted $\pi^-p \rightarrow \pi^- \pi^+ n$ data events displayed in ϕ_{TY} bins of 10 degrees with a resolution of ~ 2 degrees. The following cuts have been applied: $0.68 < MM^2 < 1.0 \text{ GeV}^2$, probability ($\pi^-p \rightarrow \pi^- \pi^+ n$) $>$ twice the probability ($\pi^-p \rightarrow \pi^- p \pi^0$), probability ($\pi^-p \rightarrow K^- K^+ n$) $<$ 30%, $M_{\pi\pi} < 0.7 \text{ GeV}$, and $(\Delta')^2 < 8\mu^2$. A weighted event corresponds to $0.012 \mu\text{b}$.

at $\Delta^2 = 0$. Figure 9 is a plot of the extrapolated cross section $(\Delta^2/\mu^2) \sigma_i$ for this case, with the use of the form factor, FF_{BD} .

2. Fit to the extrapolated on-mass-shell $\pi\pi$ cross sections using a standard scattering length formulation

The total cross section $\sigma_{\pi\pi}$ may be written as the sum of S -, P -, and D -wave cross sections, where

$$\sigma_i = \frac{4\pi}{k^2} (2l+1) \left[\frac{4}{9} \sin^2 \delta_i^0 + \frac{1}{9} \sin^2 \delta_i^2 + \frac{4}{3} \sin \delta_i^0 \sin \delta_i^2 \cos(\delta_i^0 - \delta_i^2) \right] \quad (7)$$

for the S and D waves ($l=0$ and $l=2$) and

$$\sigma_i = \frac{4\pi}{k^2} (2l+1) \sin^2 \sigma_i^1 \quad (8)$$

for the P wave ($l=1$). For this analysis the $l=0$ and 2 phase shifts were parameterized as

$$k \cot \delta_0^l = \frac{1}{a_l} + 0.5k^2 r_l \quad (9)$$

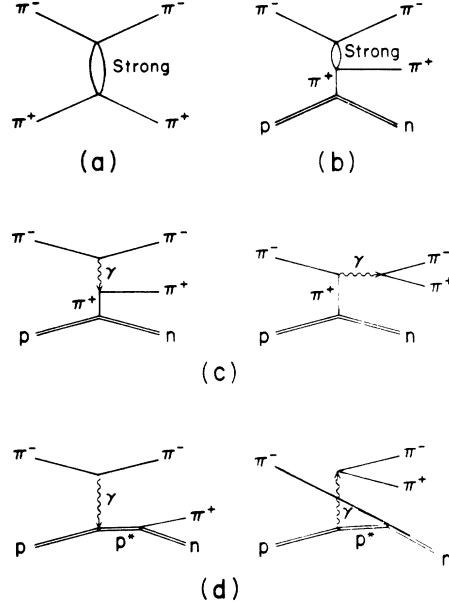


FIG. 7. Diagrams for various amplitudes discussed in the text.

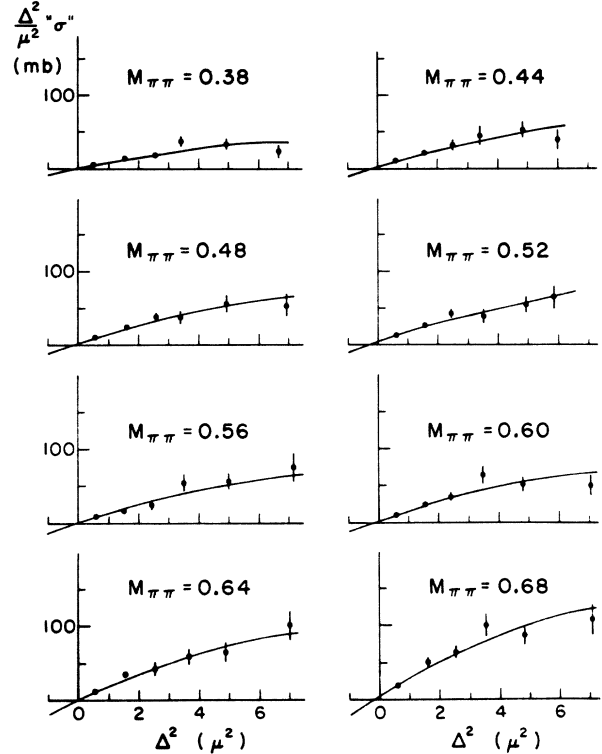


FIG. 8. Values for $(\Delta^2/\mu^2) \sigma_i$ obtained by applying the Chew-Low equation (1) to our data. The mean value of $M_{\pi\pi}$ is indicated for each of the eight $M_{\pi\pi}$ bins shown. The curves are the results of fitting the $\alpha + \beta x$ form described in Eq. (5) of the text. Values for the curve at $\Delta^2 = -1\mu^2$ and $\Delta^2 = 0$, as well as the χ^2 for these fits, are given in Table III.

TABLE III. Summary of the $\pi^- \pi^+$ extrapolations.

$\langle M_{\pi\pi} \rangle$ (GeV)	Chew-Low OPE			(Chew-Low OPE) FF_{BD}		
	$\alpha + \beta\Delta^2$	$\beta\Delta^2$	$\alpha + \beta x$	$\alpha + \beta\Delta^2$	$\beta\Delta^2$	$\alpha + \beta x$
	$\sigma_{\pi\pi}$ (mb)					
0.38	3.1±1.7	7.3±0.6	8.2±2.3	12.8±2.8	12.9±1.1	21.5±3.8
0.44	1.6±3.6	11.3±1.1	10.4±4.9	18.4±6.0	20.5±1.9	34.2±8.2
0.48	3.3±3.1	12.8±1.1	11.9±4.2	19.6±5.1	22.9±1.8	34.6±6.9
0.52	1.6±3.5	13.5±1.0	10.9±4.7	19.3±5.7	24.3±1.8	36.0±7.6
0.56	5.5±3.2	12.4±1.0	13.2±4.3	19.5±5.1	20.5±1.6	31.1±6.8
0.60	3.2±3.1	12.6±1.0	12.8±4.2	21.0±5.1	22.9±1.7	37.6±6.9
0.64	8.6±3.5	16.6±1.1	20.5±4.7	30.7±5.6	28.8±1.9	51.5±7.6
0.68	6.9±4.7	22.8±1.4	24.8±6.3	39.9±7.6	41.2±2.5	72.3±10.5
	χ^2 for extrapolations					
0.38	10.1	16.8	6.4	5.1	5.1	4.3
0.44	6.1	14.0	3.3	2.2	2.3	1.2
0.48	4.0	14.4	1.6	0.9	1.4	1.0
0.52	3.3	15.8	1.5	0.9	1.8	1.4
0.56	2.6	7.7	4.3	6.2	6.3	11.0
0.60	8.8	18.8	5.0	3.7	3.8	3.1
0.64	3.1	9.0	1.8	1.7	1.8	3.3
0.68	9.6	22.4	4.7	3.0	3.0	2.2
Total/NDF	47.6/32 ^c	118.9/40 ^o	28.6/32 ^o	23.7/32 ^o	25.5/40 ^o	27.5/32 ^o
	Δ^2 "σ" (mb) at $\Delta^2=0$					
0.38	2.7±1.1	0.0	1.2±1.2	0.1±1.5	0.0	2.2±1.7
0.44	6.6±2.3		3.6±2.7	1.3±3.4		3.6±4.0
0.48	6.4±2.0		3.8±2.2	1.9±2.8		2.1±3.2
0.52	8.2±2.3		5.1±2.6	3.0±3.3		1.9±3.8
0.56	4.5±2.0		2.2±2.2	0.6±2.8		2.4±3.2
0.60	6.4±2.0		3.3±2.3	1.1±2.9		3.6±3.3
0.64	5.4±2.2		1.8±2.5	-1.1±3.1		6.8±3.6
0.68	11.0±3.1		5.1±3.5	0.8±4.4		8.8±5.1

for $l=0$, and

$$\delta_2^l = b_l k^5 \quad (10)$$

for $l=2$, where a_l is a scattering length, r_l is an effective range, b_l is the D -wave scattering parameter, and $\hbar k$ is the pion momentum in the dipion rest frame. For the $I=1$ P -wave phase shift, δ_1^1 , we used the parameterization⁹

$$\tan \delta_1^1 = \frac{M_\rho \Gamma(M_{\pi\pi})}{M_\rho^2 - M_{\pi\pi}^2}, \quad (11)$$

where M_ρ is 0.765 GeV, and $\Gamma(M_{\pi\pi})$ is given by

$$\Gamma(M_{\pi\pi}) = \left(\frac{k}{k_\rho}\right)^3 \Gamma_1, \quad (12)$$

where k_ρ is 0.356 GeV/ c . The linear-fit parameter Γ_1 is used to fit the magnitude of the $l=1$ phase shifts in the low-energy region.

Values for a_0 , b_0 , r_0 , and Γ_1 were determined by fitting Eqs. (7) and (8) to the extrapolated $\pi\pi$ cross sections using the parameterizations given

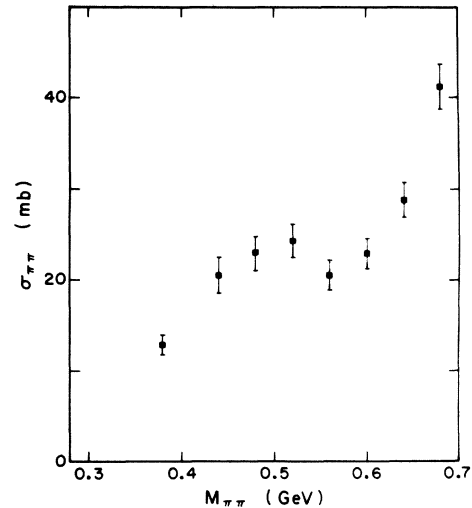


FIG. 9. The total elastic $\pi^- \pi^+ \rightarrow \pi^- \pi^+$ cross section, $\sigma_{\pi\pi}$, from extrapolation to the mass shell using the functional form Δ^2 "σ" = $\beta\Delta^2$ with FF_{BD} .

TABLE IV. Best-fit parameters from extrapolated on-shell cross sections.

Functional form	a_0 (F)	r_0 (F)	Γ_1 (GeV)	b_0 (deg/GeV ⁵)
" σ_1 "	$0.55^{+0.10}_{-0.03}$	-0.4 ± 0.5	$0.070^{+0.002}_{-0.010}$	400 ± 5600
" σ_{i1} "	$0.25^{+0.40}_{-0.08}$	$-1.8^{+4.9}_{-0.8}$	$0.010^{+0.060}_{-0.000}$	400 ± 5200
" σ_{i11} "	$0.45^{+0.40}_{-0.30}$	$-1.0^{+1.8}_{-0.9}$	$0.070^{+0.038}_{-0.030}$	400 ± 9000

in Eqs. (9) through (12). The values used for the $l=2$ parameters were those obtained in our earlier study¹ of $\pi^+p \rightarrow \pi^+\pi^+n$. The results of this fitting procedure which are given in Table IV serve as a consistency check on the results we obtained by fitting the angular distributions in Sec. III C below.

C. $\pi^-\pi^+ \rightarrow \pi^-\pi^+$ angular distributions off the mass shell

In order to obtain information on the signs of the $l=0$ and $l=2$ phase shifts we fit the $\cos\theta_J$ distributions displayed in Table II and Fig. 10 without extrapolating to $\Delta^2 = -\mu^2$. We assumed that the shapes of the on-mass-shell angular distributions are the same as the off-mass-shell data and that their magnitudes are approximated by the Chew-Low formula, Eq. (1). In order to improve this approximation we restricted the data sample for this phase of the analysis to the region $(\Delta')^2 < 4\mu^2$.

The $\pi\pi$ differential cross section is given by

$$d\sigma_{\pi\pi}/d\Omega(\theta_J) = |F(\theta_J)|^2, \quad (13)$$

where $F(\theta_J)$ was constructed by taking contributions from all diagrams to the same order as the examples given in Figs. 7(b)–7(d). It is given by

$$F(\theta_J) = [F_n(\theta_J) + f_c(\theta_J)]e^{\delta}, \quad (14)$$

where $F_n(\theta_J)$ is the strong-interaction amplitude. The gauge-invariant Coulomb amplitude, $f_c(\theta_J)$, and the real part of the radiative correction, δ , were taken from Chen and Cushing.¹⁰ The imaginary part of the radiative correction was neglected since the correction is significant only very near threshold,¹⁰ that is, for $\hbar k < 5\text{MeV}/c$. The strong-interaction amplitude was expanded in partial waves as

$$F_n(\theta_J) = \frac{1}{2ik} \sum_{l=0}^2 (2l+1) A_l P_l(\cos\theta_J), \quad (15)$$

where

$$A_l = \frac{1}{3} [\exp(2i\delta_l^0) - 1] + \frac{2}{3} [\exp(2i\delta_l^2) - 1] \quad (16)$$

for $l=0$ and 2 and

$$A_l = \exp(2i\delta_l^1) - 1 \quad (17)$$

for $l=1$. In the expression for F_n , $\hbar k$ was taken to be the momentum of a pion in the final state of the dipion system, and the phase shifts were parameterized as in Eqs. (9)–(12).

We fitted Eq. (13) to the data in Table II and Fig. 10 and obtained a χ^2 of 193 for 116 degrees of freedom. Better fits were obtained using functional forms for $\Gamma(M_{\pi\pi})$ other than that given in Eq. (12). The expression for $\Gamma(M_{\pi\pi})$ was modified to

$$\Gamma(M_{\pi\pi}) = \frac{g(M_{\pi\pi})}{g(M_\rho)} \left(\frac{k}{k_\rho}\right)^3 \Gamma_1, \quad (18)$$

where the different forms for $g(M)$ investigated are listed in Table V along with the results of the

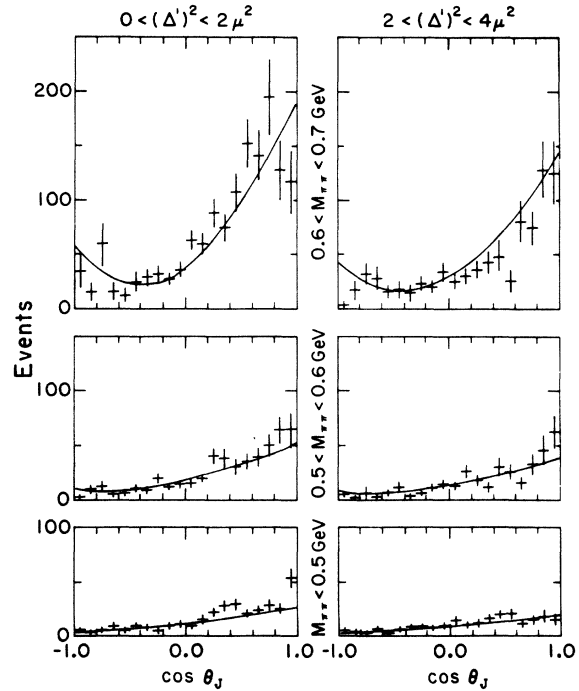


FIG. 10. Off-shell $\cos\theta_J$ distributions for the $\pi^-p \rightarrow \pi^-\pi^+n$ data weighted by the factors in Table I, and displayed in bins of 0.1. The cuts in $M_{\pi\pi}$ and $(\Delta')^2$ for each of the six plots are indicated in the figure. The curves are the fit to the data using Eqs. (13) and (14).

TABLE V. Summary of fits to the $\pi^- \pi^+ \rightarrow \pi^- \pi^+$ angular distributions off the mass shell for different choices of the functional form of $\Gamma(M_{\pi\pi})$.

Functional form for $g(M)$	References	χ^2 for 116 D.F.	a_0 (F)	r_0 (F)	b_0 (deg/GeV ⁵)	Γ_1 (GeV)
1. 1	12	193.4	$+0.49^{+0.11}_{-0.05}$	$-0.93^{+0.62}_{-0.32}$	450 ± 1700	$+0.100^{+0.020}_{-0.025}$
2. $(M)^{-1}$	9	166.1	$+0.49^{+0.11}_{-0.07}$	$-0.93^{+0.55}_{-0.39}$	450 ± 1600	$+0.080^{+0.020}_{-0.015}$
3. $(M)^{-2}$	This paper	141.4	$+0.49^{+0.08}_{-0.06}$	$-0.93^{+0.42}_{-0.23}$	400 ± 1600	$+0.070 \pm 0.010$
4. $(k^2 + k_\rho^2)^{-1}$	9	170.1	$+0.49^{+0.11}_{-0.05}$	$-0.93^{+0.55}_{-0.38}$	450 ± 1700	$+0.080^{+0.020}_{-0.015}$
5. $[M(1 + R^2 k^2)]^{-1}$	11	158.0	$+0.49^{+0.11}_{-0.05}$	$-0.93^{+0.55}_{-0.38}$	400 ± 1600	$+0.080^{+0.010}_{-0.015}$

fitting. For example, the energy variation of $\Gamma(M_{\pi\pi})$ from lowest-order perturbation theory⁹ has the form $g(M) = (M)^{-1}$. This factor increases the P -wave contribution in the lower mass regions while still retaining the resonance behavior for

$\Gamma(M_{\pi\pi})$ near the ρ mass region and improves the fit. Pišút and Roos¹¹ have used a penetration form factor, $g(M) = [M(1 + R^2 k^2)]^{-1}$, where $k^2 = (M/2)^2 - \mu^2$ and R is the radius of interaction, with $R^2 = 2.3$ (GeV)². This form yielded an even lower χ^2 .

TABLE VI. Scattering lengths from experimental determinations and theoretical models.

a_0 (μ^{-1})	a_2 (μ^{-1})	References
(a) Experiment		
	0.052 ± 0.005	Baton ¹³
$0.36^{+0.11}_{-0.20}$	$-0.036^{+0.037}_{-0.034}$ ^a	Scharenguivel ¹⁴
$0.55^{+0.50}_{-0.38}$	-0.27 ± 0.04 ^a	Scharenguivel ¹⁴
0.55 ± 0.27		Zylbersztejn ¹⁵
0.17 ± 0.13		Beier ¹⁶
0.16	-0.048	Skuja ¹⁷
0.60	0.043	
0.15	-0.05 ± 0.01	Braun ¹⁸
$0.35^{+0.06}_{-0.04}$	$-0.16^{+0.02}_{-0.03}$ ^a	Notre Dame-ANL
(b) Theory		
0.16	-0.045	Weinberg ¹⁹
0.20	-0.058	Goldberger-Treiman relation ²⁶
0.17	-0.045	Lovelace ²⁰
0.80	0.1	Fulco ²¹
0.80	0.26	Castoldi ²²
-0.5	0.2	Pišút ²³
-0.013	-0.015	
$-0.1 \leq a_0 \leq 0.8$	$-0.2 \leq a_2 \leq 0.15$	Basdevant ²⁴
$0.17 \leq a_0 \leq 0.24$	$-0.044 \leq a_2 \leq -0.041$	Morgan ²⁵
0.15 ± 0.07	-0.053 ± 0.028	Pennington ²⁷
0.24	-0.06	Franklin ²⁸
0.26 ± 0.08	-0.041 ± 0.016	Tryon ²⁹

^a This value of a_2 was used for the determination of a_0 but not measured in the reference listed.

However, the best χ^2 in Table V was obtained with $g(M)=M^{-2}$. It can be seen from Table V that variations in $\Gamma(M_{\pi\pi})$ affect the values of Γ_1 but have no effect on a_0 and r_0 . The best fit ($\chi^2=141$ for 116 degrees of freedom) for the off-shell data used the form $g(M)=M^{-2}$ and gave the following values for a_0 , r_0 , Γ_1 , and b_0 :

$$a_0 = +0.49^{+0.08}_{-0.06} \text{ F} = +(0.35^{+0.06}_{-0.04})\mu^{-1},$$

$$r_0 = -0.93^{+0.42}_{-0.23} \text{ F} = -(0.66^{+0.30}_{-0.16})\mu^{-1},$$

$$\Gamma_1 = +0.070 \pm 0.010 \text{ GeV},$$

$$b_0 = +400 \pm 1600 \text{ deg/GeV}^5.$$

A similar fit was made in which a_0 was constrained to be negative. The resulting χ^2 of 358 for 116 degrees of freedom rules out a negative value for a_0 , independent of the sign for r_0 . On the other hand, reversing the negative signs of a_2 and b_2 only changed the χ^2 of the best fit from 141 to 156, thus indicating a slight preference for negative values^{1,12} of a_2 and b_2 .

Table VI lists the values for a_0 and a_2 from this

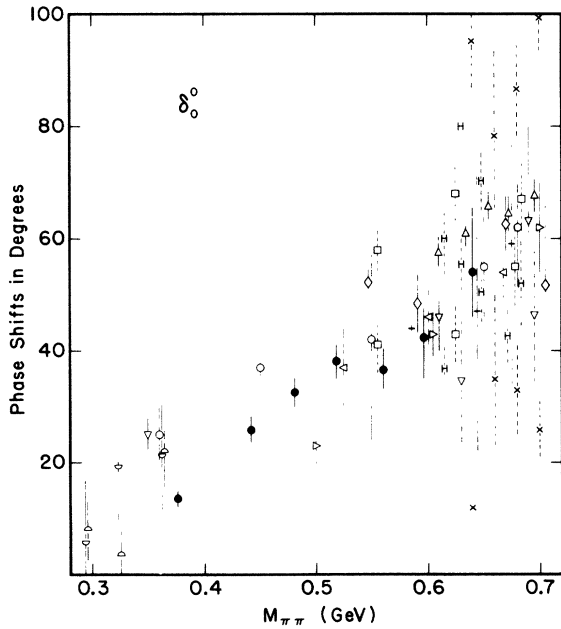


FIG. 11. The $I=0$ S -wave phase shift δ_0^0 from our essentially energy-independent analysis is indicated by closed circles, \bullet . The other available values for δ_0^0 from several experiments are presented for comparison. \times Gutay *et al.* (Ref. 30); \circ Walker *et al.* (Ref. 31); \triangleleft Baton *et al.* (Refs. 5 and 13); \triangleright Marateck *et al.* (Ref. 32); ∇ Scharenguivel *et al.* (Ref. 33); \diamond Baillon *et al.* (Ref. 34); \triangle Hyams *et al.* (Ref. 35); \square Protopopescu *et al.* (Ref. 36); $+$ Carroll *et al.* (Ref. 37); H Malamud *et al.* (Ref. 38); \triangle Beier *et al.* (Ref. 16); ∇ Zylbersztejn *et al.* (Ref. 15); and \bullet Notre Dame-ANL (this paper). Points with broken-line error bars indicate more than one solution.

and other experiments¹³⁻¹⁸ as well as values from theoretical models.¹⁹⁻²⁹ Our results are in good agreement with other experimental determinations.

D. Direct determination of δ_0^0 from the extrapolated on-mass-shell $\pi\pi$ cross sections

The $I=0$ S -wave phase shift can be determined directly from the extrapolated cross sections listed in Table III. For each $M_{\pi\pi}$ bin the total $\pi\pi$ cross section can be written as a sum of the S -, P -, and D -wave contributions, $\sigma_{\pi\pi} = \sigma_0 + \sigma_1 + \sigma_2$ with σ_0 being the dominant term at low $M_{\pi\pi}$. The sum $\sigma_1 + \sigma_2$ is determined from the values Γ_1 , b_0 , and b_2 . Subtracting $\sigma_1 + \sigma_2$ from $\sigma_{\pi\pi}$ (Fig. 9) gives the S -wave contribution to the cross section, σ_0 . This in turn is a function of only δ_0^0 and δ_0^2 , with the major contribution coming from δ_0^0 . The minor contribution from δ_0^2 was obtained using a smooth curve fit to the values for the δ_0^2 phase shifts de-

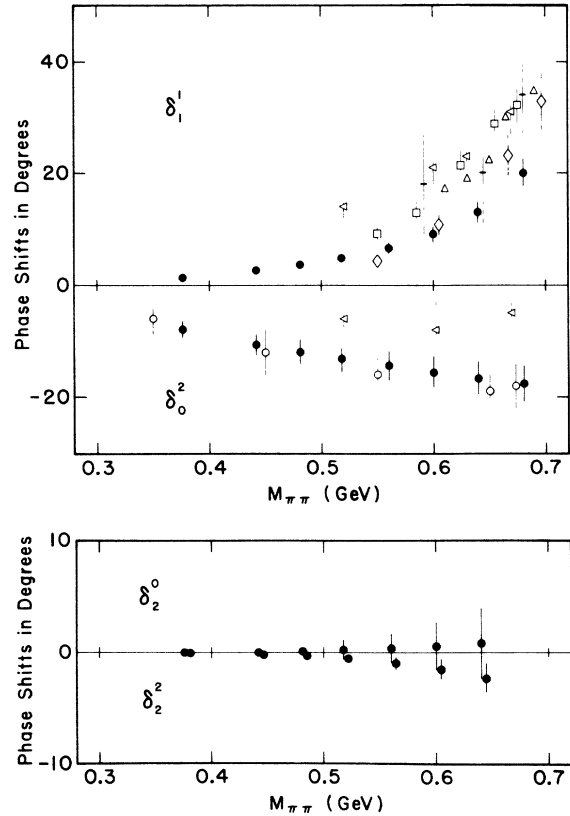


FIG. 12. Phase shifts that have been used by us and by other experimenters in order to obtain the $I=0$ S -wave phase shift δ_0^0 in Fig. 11. The notation is δ_1^1 , where I is the isospin and J is the angular momentum δ_1^1 , δ_0^0 , δ_2^2 , and δ_2^2 appear in order from top to bottom. The symbols and references are identical to those in Fig. 11, except the closed circles which are from Ref. 1 as well as this paper.

terminated from our earlier work.¹ Thus a δ_0^0 was obtained for each $M_{\pi\pi}$ bin. Our results for this essentially energy-independent determination of δ_0^0 are presented as closed circles in Fig. 11 along with other experimental results.^{13,15,16,30-38} Figure 12 shows the δ_1^1 , δ_2^2 , δ_0^0 , and δ_2^2 phase shifts used in our calculation of δ_0^0 as well as the phase shifts used by other experimenters^{13,30,31} in their determination of δ_0^0 .

A scattering length fit, Eq. (9), to our δ_0^0 phase-shift data is shown as a solid line in Fig. 13. There are several theoretical approaches to extrapolate from below threshold into the physical region. Symmetrized forward dispersion relations are used by Franklin²⁸ to provide a unitary extrapolation of the Weinberg current-algebra amplitudes. Tryon²⁹ uses twice-subtracted dispersion relations with a one-parameter model for the phase shifts. Basdevant *et al.*²⁴ and Pennington and Protopopescu²⁷ use integral equations with crossing, unitarity, and analyticity requirements. The curves from each of these different approaches which were fitted to earlier δ_0^0 data are presented in Fig. 13. The slope of these curves at threshold is the scattering length, since we have plotted the phase shifts as a function of k . All of these approaches fit our data reasonably well within errors on their curves. It would appear from this figure that the scattering length is more sensitive to the details of theoretical approach than to the present data.

IV. SUMMARY

Data from the reaction $\pi^- p \rightarrow \pi^- \pi^+ n$ were related to $\pi^- \pi^+ \rightarrow \pi^- \pi^+$ scattering via the Chew-Low formula and on-shell $\pi^- \pi^+$ cross sections were obtained. The effects of including the Benecke-Dürr form factor and the technique of conformal mapping were studied. The $\pi\pi$ cross sections were used to determine the δ_0^0 phase shifts as a function of $M_{\pi\pi}$. Scattering length parameters describing low-energy $\pi\pi$ interactions were determined from fits to the off-shell $\pi^- p \rightarrow \pi^- \pi^+ n$ angular distributions. Our results are compared with other experimental results and various theoretical interpretations.

ACKNOWLEDGMENTS

We wish to thank John Meyers and Dr. Victor Bierman for their efforts in the initial states of

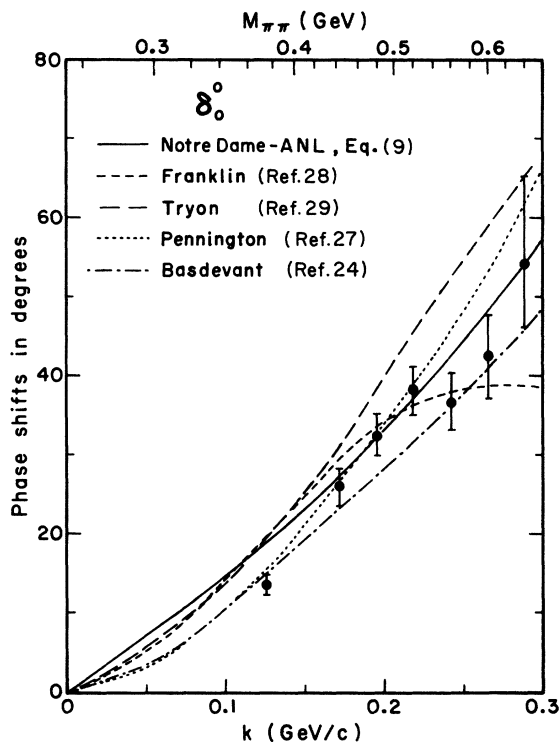


FIG. 13. Our scattering length parameterization (solid line) is compared with the shape of curves from several theoretical models which were fitted to earlier δ_0^0 data. In the case of Pennington and Protopopescu (see Ref. 17) we have averaged their bounds; in the case of Basdevant, Froggatt, and Petersen (see Ref. 24) we have used the curve from their solution No. 2. Our data from Fig. 11 are shown.

the experiment, and George Theodosiou for help during the runs; William Rickhoff and Ron Erichsen for their aid in the construction and data-taking stages; Alex Horvath and the staff of the Notre Dame machine shop; and Dr. Bruce Cork and the Argonne ZGS staff, especially Chester Brzegowy. During the analysis phase much assistance was given by Dr. Paul Kirk, our colleagues at Michigan State University, and Brian Walsh and the staff of the Notre Dame Computing Center. We wish to thank the following for their contributions to our understanding and analysis of this experiment: the theorists at Notre Dame, especially Dr. Brian Chen, Dr. James Cushing, Dr. Walter Johnson, and Dr. Paul DeCelles; also Dr. Paul Tsai and Dr. Sydney Drell from SLAC.

- *LAMPF, Los Alamos, New Mexico 87544.
- † Fermi National Accelerator Laboratory, P. O. Box 500, Batavia, Illinois, 60510.
- ‡ NMCSSC-DCA, Pentagon, Washington, D. C.
- § Physics Department, University of California, Los Angeles, California 90024.
- || Work supported in part by the National Science Foundation.
- ¶ Work supported by the U. S. Atomic Energy Commission.
- ¹J. P. Prukop, O. R. Sander, J. A. Poirier, C. A. Rey, A. J. Lennox, B. C.-j. Chen, N. N. Biswas, N. M. Cason, V. P. Kenney, and W. D. Shephard, *Phys. Rev. D* **10**, 2055 (1974).
- ²D. E. Fries, SLAC Report No. SLAC-99, 1969 (unpublished).
- ³I. Derado and R. Leedy, SLAC Report No. SLAC-72, 1967 (unpublished).
- ⁴G. F. Chew and F. E. Low, *Phys. Rev.* **113**, 1640 (1959).
- ⁵J. P. Baton, G. Laurens, and J. Reigner, *Phys. Lett.* **33B**, 525 (1970); **33B**, 528 (1970).
- ⁶R. E. Cutkosky and B. B. Deo, *Phys. Rev.* **174**, 1859 (1968).
- ⁷S. Ciulli, *Nuovo Cimento* **61A**, 787 (1969); **62A**, 301 (1969).
- ⁸J. Benecke and H. P. Dürr, *Nuovo Cimento* **56A**, 269 (1968).
- ⁹J. D. Jackson, *Nuovo Cimento* **34**, 1644 (1964).
- ¹⁰B. C.-j. Chen and J. T. Cushing, *Phys. Rev. D* **10**, 113 (1974).
- ¹¹J. Pišút and M. Roos, *Nucl. Phys.* **B6**, 325 (1968).
- ¹²J. P. Prukop, Ph.D. thesis, Univ. of Notre Dame, 1973 (unpublished).
- ¹³J. P. Baton, G. Laurens, and J. Reigner, *Nucl. Phys.* **B3**, 349 (1967).
- ¹⁴J. H. Scharenguivel, L. J. Gutay, D. H. Miller, F. T. Meiere, and S. Marateck, *Nucl. Phys.* **B22**, 16 (1970).
- ¹⁵A. Zylbersztejn, P. Basile, M. Bourquin, J. P. Boymond, A. Diamant-Berger, P. Extermann, P. Kunz, R. Mermod, H. Suter, and R. Turlay, *Phys. Lett.* **38B**, 457 (1972).
- ¹⁶E. W. Beier, D. A. Buchholz, A. K. Mann, S. H. Parker, and J. B. Roberts, *Phys. Rev. Lett.* **30**, 399 (1973).
- ¹⁷A. Skuja, M. A. Wahlig, T. B. Risser, M. Pripstein, J. E. Nelson, I. R. Linscott, R. W. Kenney, O. I. Dahl, and R. B. Chaffee, *Phys. Rev. Lett.* **31**, 653 (1973).
- ¹⁸K. J. Braun and D. B. Cline, *Phys. Rev. D* **8**, 3794 (1973).
- ¹⁹S. Weinberg, *Phys. Rev. Lett.* **17**, 616 (1966).
- ²⁰C. Lovelace, *Phys. Lett.* **28B**, 264 (1968); in *Proceedings of the Conference on $\pi\pi$ and $K\pi$ Interactions, 1969*, edited by F. Loeffler and E. D. Malamud (Argonne National Laboratory, Argonne, Ill., 1969), p. 562.
- ²¹J. R. Fulco and D. Y. Wong, *Phys. Rev. Lett.* **19**, 1399 (1967).
- ²²P. Castoldi, *Nucl. Phys.* **B12**, 567 (1969).
- ²³J. Pišút, *Nucl. Phys.* **B8**, 159 (1968).
- ²⁴J. L. Basdevant, C. D. Froggatt, and J. L. Petersen, *Phys. Lett.* **41B**, 178 (1972).
- ²⁵D. Morgan and G. Shaw, *Phys. Rev. D* **2**, 520 (1970).
- ²⁶M. Goldberger and S. B. Treiman, *Phys. Rev.* **110**, 1178 (1958).
- ²⁷M. R. Pennington and S. D. Protopopescu, *Phys. Rev. D* **7**, 1429 (1973).
- ²⁸J. Franklin, *Phys. Rev. D* **11**, 513 (1975).
- ²⁹E. P. Tryon, *Phys. Rev. D* **10**, 1595 (1974).
- ³⁰L. J. Gutay, P. B. Johnson, F. J. Loeffler, R. L. McIlwain, D. H. Miller, R. B. Willmann, and P. L. Csonka, *Phys. Rev. Lett.* **18**, 142 (1967).
- ³¹W. D. Walker, J. Carroll, A. Garfinkel, and B. Y. Oh, *Phys. Rev. Lett.* **18**, 630 (1967).
- ³²S. Marateck, V. Hagopian, W. Selove, L. Jacobs, F. Oppenheimer, W. Schultz, L. G. Gutay, D. H. Miller, J. Prentice, E. West, and W. D. Walker, *Phys. Rev. Lett.* **21**, 1613 (1968).
- ³³J. H. Scharenguivel, L. J. Gutay, D. H. Miller, L. D. Jacobs, R. Keyser, D. Huwe, E. Marquit, F. Oppenheimer, W. Schultz, S. Marateck, J. D. Prentice, and E. West, *Phys. Rev.* **186**, 1387 (1969).
- ³⁴P. Baillon, R. K. Carnegie, E. E. Kluge, D. S. G. S. Leith, H. L. Lynch, B. Ratcliff, B. Richter, H. H. Williams, and S. H. Williams, *Phys. Lett.* **38B**, 555 (1972).
- ³⁵B. Hyams, C. Jones, P. Weilhammer, W. Blum, H. Dietl, G. Grayer, W. Koch, E. Lorenz, G. Lütjens, W. Männer, J. Meissburger, W. Ochs, U. Stierlin, and F. Wagner, *Nucl. Phys.* **B64**, 134 (1973).
- ³⁶S. D. Protopopescu, M. Alston-Garnjost, A. Barbaro-Galtieri, S. M. Flatté, J. H. Friedman, T. A. Lasinski, G. R. Lynch, M. S. Rabin, and F. T. Solmitz, *Phys. Rev. D* **7**, 1279 (1973).
- ³⁷J. T. Carroll, J. A. J. Matthews, W. D. Walker, M. W. Firebaugh, J. D. Prentice, and T. S. Yoon, *Phys. Rev. D* **10**, 1430 (1974).
- ³⁸E. Malamud and P. E. Schlein, *Phys. Rev. Lett.* **19**, 1056 (1967).